# FINDING ROUTES FOR EFFICIENT AND SUCCESSFULL SLOPE ASCENT FOR EXPLORATION ROVERS

*Hiroaki Inotsume[1], Colin Creager[2], David Wettergreen[1], William "Red" Whittaker[1]

[1]*Carnegie Mellon University, 5000 Forbes Avenue, Pittsburgh, Pennsylvania 15213, USA,*

*E-mail: hinotsume@cmu.edu, dsw@cmu.edu, red@cmu.edu*

[2]*NASA Glenn Research Center, Mail Stop 23-3, 21000 Brookpark Road, Cleveland, Ohio 44135, USA,*
*E-mail: colin.m.creager@nasa.gov*

## ABSTRACT

This paper addresses the problem of selecting routes for ascending slopes of loose, unconsolidated soil. When exploring sloped terrain where high slippage is likely, rovers need to find efficient and successful routes because of limited energy. In this research, the influence of the rover's heading on slope, or angle of attack, on the slope ascent performance was analyzed based on an analytical rover model. The rover slip and tractive power efficiency were predicted and associated with the angle of attack. Based on the analysis, this research proposed a strategy to select feasible routes that maximize the power efficiency under user-defined slip regulation levels. Numerical simulations were demonstrated to evaluate the usability of the proposed route selection method.

## 1. INTRODUCTION

Research on navigation of ground vehicles typically examines flat or benign terrains where vehicle slippage is negligible. Otherwise routes avoid high slopes and high slip situations. These navigation algorithms are sufficiently robust for most of indoor and outdoor situations. However, sometimes we want to make robots explore challenging terrains, steep slopes of sand dunes, crest of mountains, or rims and interiors of craters where no gentle route exists and where robots need to take some risks of mobility hazard, or immobilization.

Some research, for example [1,2,3], explicitly takes into consideration the vehicle slip for planning over terrains that include inclines in some part. However none of them presents planning to overcome steep slopes where a rover can be potentially immobilized in soil.

The objective of this research is to find a route to increase the efficiency and possibility of successful slope-ascent for a rover, given its configuration, terrain geometry, and soil properties. To this end, this research analyzes the influence of the angle of attack (AoA) on slope-ascent performance of rovers.

*(a) Scarab* *(b) Andy*

*Figure 1: Scarab and Andy rovers for lunar surface exploration.*

Here the term AoA is defined as an angle of the heading of a rover with respect to the transverse direction of the slope (shown as α in Figure 2 (a)). The AoA is 90° when a rover is oriented to the uphill direction, and 0° in the lateral direction of the slope.

The influence of AoA was experimentally studied in [4] for a specific vehicle and terrain. They showed that while the lower AoAs result in lower vehicle slip and sinkage, higher power efficiency can be achieved at higher AoAs. This research further investigates these effects of AoA from different perspectives and expand the scope toward motion planning.

In this work, two lunar rover prototypes, Scarab and Andy shown in Figure 1, are studied as target vehicles to evaluate the performance of different scale of vehicles. Scarab is a large rover that has a mass of 400 kg and size of about 2 m long by 1.6 m wide in its nominal configuration. Andy, on the other hand, is a relatively light-weighted small rover whose mass is about 25 kg and the dimension is about 0.9 m long by 1.1 m wide. The specifications of the two rovers are shown in Table 1.

The analysis is made by a slope-ascent model of a rover which consists of steady state force conditions on slope and a terramechanics-based wheel–soil interaction. The model is validated through a set of slope-ascent experiments using the Scarab rover. The rover slip and tractive power efficiency are predicted

*Table 1: Specifications of Scarab and Andy. CG X and Y locations indicate the planar position of the CG w.r.t the geometrical center of the vehicle.*

| | Scarab | Andy |
|---|---|---|
| Mass | 400 kg | 25 kg |
| Wheelbase | 120 cm | 60 cm |
| Track-width | 140 cm | 80 cm |
| Wheel diameter | 71 cm | 32 cm |
| Wheel width | 18 cm | 15 cm |
| CG X location | 4 cm | 2 cm |
| CG Y location | ~ 0 cm | ~ 0 cm |
| CG height | 64 cm | 31 cm |

based on the model and associated with AoA. Moreover a strategy for selecting an efficient and successful slope-ascent route is proposed. The usefulness of the proposed strategy is demonstrated through a series of slope-ascent simulations for Scarab and Andy rovers.

## 2. SLOPE-ASCENT MODEL

The focus of this research is on linear trajectory motions to ascend slopes of deformable, slip-inducing soil. The paper does not address any aggressive steering maneuvers or curvilinear trajectories to simplify the problem. In addition, while the slope-ascent performance can be greatly improved with active posture controls as reported in **[**5**]**, this research focuses only on conventional rovers that do not have such capability. The basic ideas of this research, however, can be applicable to those outside of the scope.

We assume that the orientation of vehicles and wheels are fixed and the vehicles are commanded to drive in a straight line. The orientation errors, if any, are assumed to be negligible or kept in minimal with some appropriate orientation control. We also assume slopes of a relatively flat surface and homogeneous soil condition. While actual terrains rovers encounter are somewhat bumpy with local variations of inclination, the smooth surface representation can be considered as an approximation of terrains by a combination of best-fitted planes to the local terrains.

Under these assumptions, this section introduces a slope-ascent model of a rover. The model used in this research is twofold: a steady state rover model and a terramechanics-based wheel–soil interaction. These two models are described in Section 2.1 and 2.2, respectively.

### 2.1. Steady State Rover Model

Figure 2 illustrates a rover that climbs up a slope of angle $\theta_0$ at an AoA of $\alpha$. The rover is driven

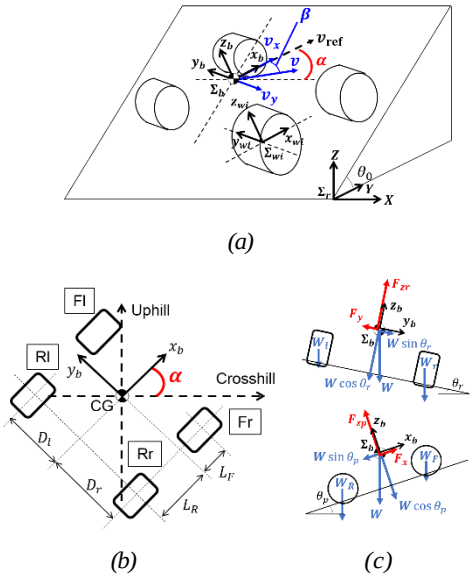


*Figure 2: Schematic view of a steady-state rover climbing slope.*

with a commanded reference velocity $v_{ref}$ in the rover heading. Due to the longitudinal and lateral slip, the rover actually travels with a velocity $v$ in the direction that deviates from the rover heading by slip angle $\beta$.

The longitudinal slip of the vehicle is measured by the slip ratio $s$:

$$s = 1 - v_x / v_{ref} \quad (1)$$

The angle $\beta$ represents the amount of the downhill sideslip. This slip angel is given as

$$\beta = \tan^{-1}\left(v_y / v_x\right) \quad (2)$$

where $v_x$ and $v_y$ denote the longitudinal and lateral velocities of the vehicle, respectively.

On the slope, the total weight of the rover $W$ is distributed to each wheel depending on the rover configuration and orientation as well as the inclination of the slope as seen in Figure 2 (c). For example, the weight distributed on the forward left wheel $W_{Fl}$ is given as

$$W_{Fl} = W \frac{L_R}{L}\frac{D_r}{D}\left(1 - \frac{H}{L_R}\tan\theta_p\right)\left(1 - \frac{H}{D_r}\tan\theta_r\right) \quad (3)$$

where $L_R$ denotes the longitudinal distance from the planer location of the center of gravity (CG) to the rear wheels whereas $D_r$ denotes the lateral distance between the CG and the right wheels as shown in Figure 2 (b). $L = L_F + L_R$ and $D = D_l + D_r$ are the wheelbase and track-width of the vehicle, respectively. $H$ is the height of the CG w.r.t the slope surface. The two angles $\theta_p$ and $\theta_r$ in Eq. (4) are the pitch and roll angles of the vehicle on the slope. These angles are determined geometrically based on the slope inclination $\theta_0$ and the vehicle AoA $\alpha$ as

follows:

$$\begin{cases} \sin\theta_p = \sin\theta_0 \sin\alpha \\ \sin\theta_r = \sin\theta_0 \cos\alpha \end{cases} \quad (4)$$

To drive up the slope in a steady state, the wheels of the vehicle must generate sufficient amount of forces to overcome the gravitational resistive force that pulls the vehicle downhill. The condition for the steady state is given in the following equations:

$$\begin{cases} \sum F_{xi} = W \sin\alpha \\ \sum F_{yi} = W \cos\alpha \\ F_{zi} = W_i \cos\theta_0 \end{cases} \quad (5)$$

where $F_{xi}$, $F_{yi}$, and $F_{zi}$ are the drawbar pull, lateral force, and vertical force, respectively, that the $i$-th wheel generates through wheel–soil interaction.

## 2.2. Wheel-Soil Interaction

In this research, the above-mentioned wheel–soil interaction forces are modeled based on the Wong–Reece terramechanics model [6]. This section briefly introduces the model. More detailed descriptions of the terramechanic models can be found in [6,7,8].

Figure 3 depicts a wheel moving in deformable soil. The wheel is experiencing the slippage in its longitudinal and lateral directions and sinks in the soil by amount $z$. Against these slippage and sinkage, the soil generates stresses on the wheel–soil contact patch in the normal, tangential, and lateral directions. The drawbar pull, lateral force, and vertical force which the wheel attains can be computed by integrating these stresses in the $x_w$, $y_w$, and $z_w$ directions, respectively:

$$\begin{cases} F_x = rb\int_{\theta_r}^{\theta_f} (\tau_t(\theta)\cos\theta - \sigma(\theta)\sin\theta)d\theta \\ F_y = rb\int_{\theta_r}^{\theta_f} \tau_l(\theta)d\theta \\ F_z = rb\int_{\theta_r}^{\theta_f} (\tau_t(\theta)\sin\theta + \sigma(\theta)\cos\theta)d\theta \end{cases} \quad (6)$$

Although some level of resistive force is generated on the sidewall of the wheel when it sideslips, this study assumes that the magnitude of that force is negligible compared to the shearing forces on the wheel cylindrical contact patch.

In addition to the interaction forces, the driving torque $T$ required to drive the wheel in soil is given as follows:

$$T = rb\int_{\theta_r}^{\theta_f} \tau_t d\theta \quad (7)$$

The normal stress distribution $\sigma(\theta)$ is modeled based on Reece's pressure–sinkage relationship as follows:

$$\sigma(\theta) = k_\sigma (r/b_w)^n (\cos\theta_f - \cos\theta^*)^n \quad (8)$$

where $k_\sigma$ and $n$ are parameters specific to the soil type, called pressure–sinkage modulus and sinkage

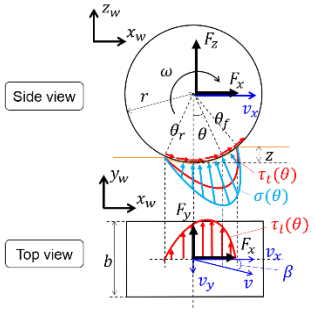


*Figure 3: Terramechanics wheel-soil interaction model.*

exponent, respectively. $r$ is the wheel radius whereas $b_w$ is the smaller dimension of the wheel–soil contact patch. $\theta^*$ is the wheel angle defined bellow to make the stress distribution symmetric at some angle $\theta_m$ where the normal stress becomes maximum:

$$\theta^* = \begin{cases} \theta & (\theta_m \le \theta \le \theta_f) \\ \theta_f - \frac{\theta_m - \theta_r}{\theta_f - \theta_r}(\theta - \theta_r) & (\theta_r \le \theta < \theta_m) \end{cases} \quad (9)$$

The location of the angle $\theta_m$ shifts forward when the wheel slip increases, and it is estimated as a liner function of the slip ratio.

On the other hand, the shear stress distributions in the tangential and lateral directions, $\tau_t(\theta)$and $\tau_l(\theta)$ respectively, are estimated based on the total shear stress $\tau(\theta)$ and the slip velocity of the soil as follows:

$$\begin{cases} \tau_t(\theta) = \tau(\theta)\cdot \frac{v_{jt}(\theta)}{\sqrt{{v_{jt}}^2(\theta) + {v_{jl}}^2(\theta)}} \\ \tau_l(\theta) = \tau(\theta)\cdot \frac{v_{jl}(\theta)}{\sqrt{{v_{jt}}^2(\theta) + {v_{jl}}^2(\theta)}} \end{cases} \quad (10)$$

where $v_{jt}(\theta)$ and $v_{jl}(\theta)$ are the slip velocity of the soil in the tangential and lateral directions. The total shear stress $\tau(\theta)$ is modeled based on the Morh–Coulomb's failure criteria and Janosi–Hanamoto's shear stress–shear displacement relationship as

$$\tau(\theta) = (c + \sigma(\theta)\tan\phi)(1 - e^{j(\theta)/k}) \quad (11)$$

where $c$ and $\phi$ denote the cohesion and internal friction angle of the soil. $j(\theta)$ is the displacement of the soil from the wheel leading edge to the angle $\theta$. $k$ is another model parameter, called shear deformation modulus.

The tangential and lateral slip velocities $v_{jt}(\theta)$ and $v_{jl}(\theta)$, respectively, in Eq. (10) are caused from the wheel rotation and sideslip motions and modeled as functions of the slip ratio $s$ and slip angle $\beta$ of the wheel as follows:

$$\begin{cases} v_{jt}(\theta) = r\omega - v_x\cos\theta = r\omega\{1-(1-s)\}\cos\theta \\ v_{jl}(\theta) = -v_y = -r\omega(1-s)\tan\beta \end{cases} \quad (12)$$

## 3. EXPERIMENTS

Slope-ascent experiments were conducted to validate the proposed slope-ascent model for analysis. Note that two terramechanic parameters, pressure–sinkage modulus $k_\sigma$ in Eq. (8) and the shear deformation modulus $k$ in Eq. (11) are treated as variables which depend on the wheel slip to capture the wheel–soil interaction at high slip. $k_\sigma$ controls the sinkage whereas $k$ affects the drawbar pull and lateral force. These parameters were tuned as functions of the slip ratio based on the slope-ascent experiments.

### 3.1 Experiment Procedures

In this set of experiments, the Scarab rover shown in Figure 1 (a) was utilized. The mass of the rover was set to 400 kg and the four rigid grouserless wheels of 71 cm (diameter) by 18 cm (width) were mounted. The rover has active suspensions which control the angles of left and right side rocker arms and thus the rover roll angle [5]; however in this study, the suspension was fixed.

Tests were conducted using an adjustable tilt bed in the Simulated Lunar Operations (SLOPE) laboratory of the NASA Glenn Research Center. The tilt bed has a length of 6 m, a width of 4.5 m, and it is filled with 0.23 m deep of GRC-1 lunar regolith simulant [9].

In the experiments, the tested slope angle was varied from 10° to 25°, and the AoA of the rover was set to 30° to 90°.

The procedures for preparing the sand pit and measuring data are same as those used in [4]. At the beginning of each test, the soil was well loosened and leveled. Then the angle of the tilt table was set to the desired slope angle. The rover was then placed with the target AoA (α in Figure4).

After the placement, the rover was commanded to drive straight up a slope at the AoA for 30 seconds. All of the wheels were driven equally with a linear speed of 4.5 cm/s at zero slip. During each test, the motion of the rover was tracked using a stereo camera. The pair of cameras captured stereo images of the target markers on the left front and rear wheels of the rover every 2 seconds. The three-dimensional positions of the wheels at each time frame were computed offline with respect to the fixed reference coordinate markers. From the trajectory extracted, the average rover velocity in the body frame was calculated for each time step. Then the average vehicle slippage was estimated from the data points after the vehicle motion got in a steady state (typically 15–20 seconds after the vehicle starts driving).

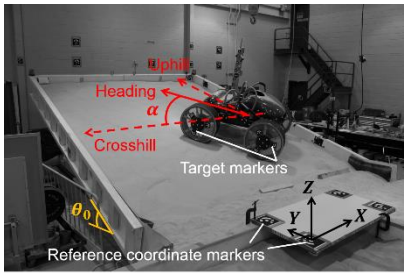


*Figure 4: Slope-ascent test setup.*

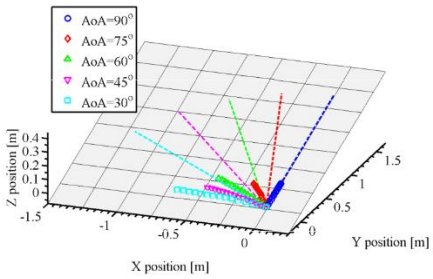


*Figure 5: Example vehicle trajectories on 15° slope. The dashed lines represent the commanded trajectories and the markers show the actual trajectories during the experiments with an interval of 2 sec.*

### 3.2 Experiment Results

The rover trajectories on 15° slope measured in the experiments are shown in Figure 5. In the figure, the dashed lines indicate the commanded trajectories while the markers represent the actual rover trajectories plotted at an interval of 2 sec. As seen in the figure, the longitudinal progresses of the rover were shorter than the length of the commanded trajectories due to the longitudinal slip, and the rover trajectories deviated from the commanded lines toward the downhill direction due to the lateral slip. It can be also seen that the shallower angles of attack could travel longer distances because of lower slip ratios.

The slip ratio and slip angle estimated from the experiments are plotted in Figures 6 (a) and (b) together with those predicted based on the analytical model. As mentioned, the two parameters, pressure–sinkage modulus $k_\sigma$ and shear deformation modulus $k$, were tuned as functions of the wheel slip ratio $s$ so that the errors between the model curves and the experimentally measured slip and sinkage were minimized. The obtained functions for the two parameters are as follows:

$$k_\sigma = 8.65\, e^{-1.98s} \times 10^5 \quad (\mathrm{N}/m^2)$$

$$k = -0.348s^2 + 0.412s + 0.013 \quad (\mathrm{m})$$

Note that there is no physical reasoning for the representations. Table 2 lists some other model parameters used in the computation.

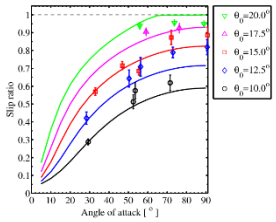


*(a) Slip ratio*

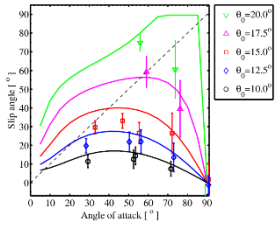


*(b) Slip angle*

*Figure 6: Measured (markers) and predicted (solid curves) slip for various AoAs and slopes. Dashed lines indicate the slip levels on/above which the rover fails slope ascent.*

*Table 2: Terramechanics parameters. Parameters were adopted from [9]*

| Parameter | Value |
|---|---|
| Soil cohesion, $c$ | 500 Pa |
| Internal friction angle, $\phi$ | 33.7° |
| Sinkage exponent, $n$ | 1.23 |

As shown in Figure 6 (a), the measured slip ratio basically decreases along with the AoA. The model-predictive curves of the slip ratio show a good agreement with this trend. When the AoA decreases from 90°, the predicted slip angle rises at first, reaches highest, and then turns to gradual reductions as the AoA further decreases as seen in Figure 6 (b). The slip angle from the experiments somewhat shows this trend. Notice that the predicted slip angle tends to be larger than that observed in the experiments. The overestimate of the slip means the prediction is on the safe side.

Overall, the model predictions agree with the experimentally observed tendencies. This fact validates the utility of the proposed model.

# 4 MODEL-BASED ANALYSIS

This section analyzes the performance of the two rovers, Scarab and Andy shown in Figure 1, based on the slope-ascent rover model.

## 4.1 Evaluation Criteria

To evaluate the slope-ascent performance, three criteria are used in this research. First two criteria are the slip ratio and slip angle defined in Eqs. (1) and (2), respectively. In addition to representing the amount of velocity lost, the slip ratio also indicates the risk of immobilization.

Another criterion utilized is power efficiency of the slope-ascent motion, namely climbing efficiency. The climbing efficiency is defined as a ratio of the tractive power in the uphill direction to the electric power input to the actuators as follows:

$$\eta_Y = F_Y v_Y / P \tag{13}$$

where $F_Y$ denotes the forces that the wheels generate in the uphill direction. $F_Y$ becomes $F_Y = W \sin\theta_0$ at a steady state. $v_Y$ is the uphill directional component of the vehicle velocity, and it is given as

$$\begin{aligned} v_Y &= v_x \sin\alpha - v_y \cos\alpha \\ &= v_{ref}(1-s)\,(\sin\alpha - \tan\beta\cos\alpha) \end{aligned} \tag{14}$$

$P$ is the electric power input and can be estimated from the following equation:

$$P = T\omega/\eta_a \tag{15}$$

where $T$ denotes the wheel driving torque which is predicted from Eq. (7), and $\omega$ denotes the wheel angular velocity. $\eta_a$ is the power efficiency of the driving actuator.

## 4.2 Slope-Ascent Performance

The predicted slope-ascent performance of Scarab and Andy are shown in Figure 7. The pressure–sinkage modulus $\boldsymbol{k_\sigma}$ and shear deformation modulus $\boldsymbol{k}$ for Andy were tuned from experiments.

As seen in the figures, both the longitudinal and lateral slip increase when the slope becomes higher for both rovers. When the AoA becomes smaller than 90°, the slip ratio monotonically reduces as shown in Figure 7 (a) or (d). Therefore shallower AoA is preferable to reduce the risk of immobilization. The reduction of the longitudinal slip along with the AoA is attributed to the decrease of the longitudinal gravitational resistance when the rover heading changes from the uphill direction to the side-slope direction.

On the other hand, the model-predicted slip angle behaves in a slightly complicated way as seen in Figure 7 (b) or (e). When the AoA is 90°, no sideslip is induced since no external forces in the lateral direction act on the rover. The sideslip starts to increase when the AoA gets smaller than 90° since the lateral gravitational resistance increases along with the reduction of the AoA. At the AoA close to 90°, the slip angle increases rapidly. This is because the longitudinal slip becomes relatively high around 90° AoA. The high longitudinal slip results in large soil shearing in the wheel tangential direction, and the increase of that tangential soil shearing limits the capability of the soil togenerate the lateral shear resistance against the sideslip. Therefore, the wheel is

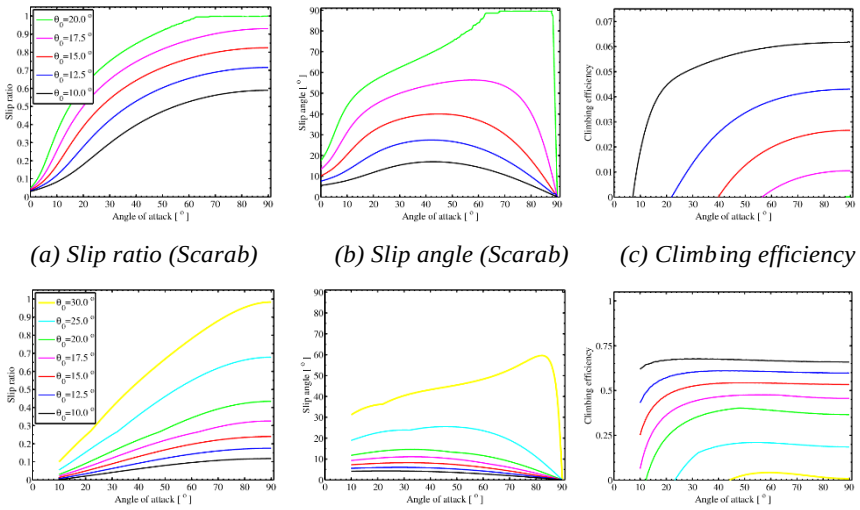


*(a) Slip ratio (Scarab)* *(b) Slip angle (Scarab)* *(c) Climbing efficiency (Scarab)*

*(d) Slip ratio (Andy)* *(e) Slip angle (Andy)* *(f) Climbing efficiency (Andy)*

*Figure 7: Slope-ascent performance of Scarab and Andy for various AoAs.*

subjected to experience relatively large sideslip around 90° AoA to generate a sufficient level of the lateral force. This causes the rapid increase of the sideslip angle at the AoA close to 90°. As the longitudinal slip and tangential shear stress reduces when the AoA further decreases, the capacity of the soil to generate lateral shear resistance recovers, and the required lateral force can be obtained with smaller slip angle. This is why the slip angle has a peak at a certain mid AoA.

The climbing efficiency of Scarab and Andy are shown in Figure 7 (c) and (f), respectively. As seen in these figures, the efficiency curves of the two rovers show quite different characteristics. The efficiency of Scarab becomes highest at 90° AoA in every slope, and it declines as the AoA reduces from 90°. This indicated that 90° direct ascent provides the most efficient uphill motion for the rover, in the tested configuration. This consists with the conclusion reported in [4]. The efficiency of Andy, on the other hand, is almost constant on 10° and 15° slopes even if the AoA is reduced from 90° until a certain angle as seen in Figure 7 (f). The efficiency suddenly drops at AoA smaller than that and eventually becomes below zero. On slopes steeper than or equal to 20°, a peak in the efficiency clearly appears at a certain AoA smaller than 90°. The difference between the maximum efficiency and that of 90° becomes more significant as the slope becomes steeper indicating the effectiveness of the diagonal slope-ascent over the direct ascent.

# 5 ROUTE SELECTION BASED ON SLIP AND EFFICIENCY

In light of the analysis in the previous section, this section presents a strategy to select a route for efficiently ascending slope.

## 5.1 Route Selection Strategy

According to the analysis, shallow AoA is preferable to reduce the longitudinal slip and thus the risk of immobilization. However, reducing the AoA can result in longer travel distance and less efficient motion due to large downhill sideslip. Therefore everything is trade-off among safety, distance, time, and power efficiency.

In this research, we propose a route selection strategy which determines a route, or AoA, that maximizes the efficiency while reducing the risk of mobility hazard. In the strategy a successful and efficient route is derived in the following two steps: 1) setting a rover slilp regulation level and 2) maximizing climbing efficiency under the slip regulation. This route selection is expressed as a simple constrained optimization problem as follows:

$$\alpha^* = \arg\max_{\alpha} \eta_Y(\alpha, s) \quad \text{subject to } s \leq s_{th} \tag{15}$$

where $\alpha^*$ denotes the selected AoA, $s$ is the slip ratio, $s_{th}$ is the threshold slip, and $\eta_Y$ is the climbing efficiency estimated from Eq. (13). The climbing efficiency was chosen for the single metric cost (or reward) function since the parameter can represent and include all aspects of travel time, distance, and total energy consumption, i.e. higher climbing efficiency means relatively shorter travel time, shorter distance, and lower energy consumption. This kind of energy-related metric is preferable since it can also reflect the roughness of the terrain (more energy required for traveling rocky or bumpy terrains) in addition to the path length [1,2] although this research assumes terrains of smooth surfaces.

### 5.2 Climbing Efficiency Diagram

This section introduces Climbing Efficiency Diagram (CED) to implement and demonstrate the proposed route selection strategy. An example CED for Andy rover on is shown in Figure 8. The CED is basically twofold: (1) an efficiency characteristic curve and (2) superimposed slip levels for the given slope. The diagram indicates comprehensive slope-ascent capability of the rover at various AoAs over the terrain, showing the climbing efficiency, slope-ascendability, and slip levels.

First, the diagram provides the information of how the efficiency changes along with the AoA. As shown in Figure 8 the climbing efficiency gently rises when the AoA reduces from 90°and reaches the highest and then it drops as the AoA gets further smaller.

Secondly, the diagram indicates the feasible AoA to ascend the slope. According to Figure 9, the AoA from 12.5° to 90° can ascend the slope as the climbing efficiency becomes positive at the AoA.

Moreover, the CED also shows the variations of the slip ratio for different AoAs. More specifically, it can be noticed from the diagram that the slip ratio is $0.1 \leq$ s at the AoA between $0^{\circ} \leq \alpha \leq 21.4^{\circ}$, the slip is $0.1 \leq s \leq 0.2$ at $21.4^{\circ} \leq \alpha \leq 36.5^{\circ}$, and so force. The width of the slip ratio band can be arbitrarily set depending on how much detail of the slip variation needs to be known.

A preferable rover heading can be found using the CED by setting an appropriate slip threshold level and then by maximizing the climbing efficiency of the motion under the regulation.

### 5.3 Route Selection Simulations

The route selection strategy proposed in Section 5.1 was demonstrated using the CED through a series of slope-ascent simulations. Routes on 15° slope for Scarab and 31° slope for Andy were determined. In the simulations, the rovers were commanded to drive up the target slopes 3 meters uphill with the selected AoAs at reference velocity of 5 cm/s.

#### 5.3.1. Scarab on 15° slope

Figure 10 (a) shows the CED for Scarab on 15° slope. The minimum slip ratio on this slope is more than 0.6 for all of the slope-ascendable AoAs. As mentioned in the previous section, the efficiency of Scarab gets highest at 90° AoA. In this simulation scenario, two slip regulation levels, $s_{th} = 0.8$ and $s_{th} = 0.95$, were set to see how different slip regulation levels result in different traversal outcomes. The corresponding AoAs that maximizes the efficiency under these slip regulations are $\alpha = 70.5^{\circ}$and $\alpha = 90^{\circ}$, respectively. The simulation results of these angles are visualized in Figure 9 (b) and summarized in Table 3. The direct ascent route could drive up the slope with 11% shorter

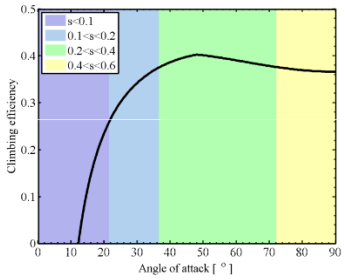


*Figure 9: Example climbing efficiency diagram.*

time, 33% shorter distance, and 6.6% less energy consumption with respect to those of the 70.5° AoA route. However the 90° AoA experienced almost 90% slip whereas the slip of the other route was kept at the selected 80% slip regulation. As this example shows, the proposed strategy can provide relatively efficient routes depending on the user's acceptable slip level.

#### 5.3.2. Andy on 31° slope

On 31° slope, Andy can no longer drive directly up the slope at 90° AoA since the slip reaches 100% and the climbing efficiency gets zero as seen in Figure 9 (c). Still however the rover can ascend the slope with some smaller AoA. The slope-ascendable AoA is very limited and rages between about 51.5°–69.5° as depicted in the figure. In addition, it can be expected that the rover experiences very high level of slip at those AoAs; the lowest slip is 0.73 at 51.5°. As the target terrain is so challenging that the rover cannot directly ascend and that significantly high slip is inevitable at any AoAs, the goal of this scenario is to derive a route which can rescue the rover from the terrain as efficiently as possible even by taking the risk of extremely high slip.

From the above observation, a slip threshold of $s_{th} = 0.95$ was set in this case. The selected AoA for this slip regulation was $\alpha = 59^{\circ}$. Figure 9 (d) visualizes the executed motion of the rover at the AoA. The simulation results are summarized in Table 4. As mentioned, the rover did not make any forward progress at all with $\alpha = 90^{\circ}$. On the other hand, while the rover requires very long transverse time and distance, it could reach the goal line with the slip ratio of 0.82 by heading the AoA derived from the proposed strategy.

## 6 CONCLUSION

This paper addressed the issue of finding efficient routes to ascend slope of deformable soil. To this end, the effect of the angle of attack (AoA) on the slope-ascent performance of rovers was analyzed based on the slope-ascent model. The analysis showed that the longitudinal slip can be reduced by decreasing the AoA, but that can cause less efficient motion. We proposed a strategy to select an efficient and successful route to overcome slope.

*Table 3: Route selection results of Scarab on 15° slope.*

| AoA | Travel time | Travel distance | Slip ratio | Slip angle | Climbing efficiency | Energy consumption |
|---|---|---|---|---|---|---|
| 90.0° | 342.8 s | 3.0 m | 0.875 | 0.0° | 0.026 | 59.7 kJ |
| 70.5° | 388.5 s | 4.5 m | 0.800 | 28.6° | 0.024 | 63.9 kJ |

*Table 4: Route selection results of Andy on 31° slope. 90.0° AoA failed the slope-ascent.*

| AoA | Travel time | Travel distance | Slip ratio | Slip angle | Climbing efficiency | Energy consumption |
|---|---|---|---|---|---|---|
| 90.0° | — | — | 1.000 | 0.0° | — | — |
| 59.0° | 3115.6 s | 49.6 m | 0.820 | 55.5° | 0.011 | 34.3 kJ |

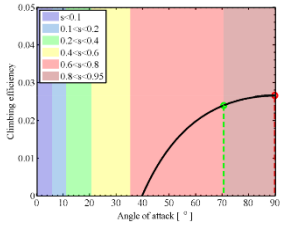


*(a) CED of Scarab on 15° slope*

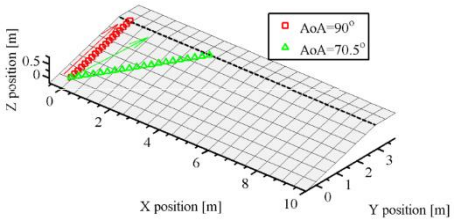


*(b) Trajectories of Scarab on 15° slope*

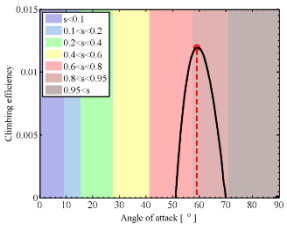


*(c) CED of Andy on 31° slope*

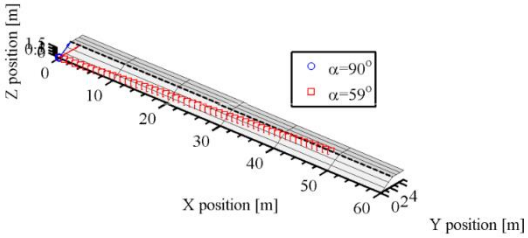


*(d) Trajectories of Andy on 31° slope*

*Figure 9: Route selection results. The AoAs highlighted in the CEDs (a) and (c) correspond to the arrows depicted in the same colors in (b) and (d). Markers in (b) and (d) are the corresponding rover trajectories.*

The proposed route selection strategy consists of the slip regulation and the climbing efficiency maximization under the slip constraints. The route selection method was implemented with the climbing efficiency diagram, and demonstrated its usefulness in numerical simulations for different rovers and for different slopes.

Currently we are planning an experimental campaign to validate the proposed route selection strategy. Incorporating the ideas developed in this research into a global/local path planner is another prospective area of future research.

## References


[1] Helmick D, et al (2009) Terrain adaptive navigation for planetary rovers. *JFR*. 26 (4): 391-410.

[2] Ishigami G, et al (2011) Path planning and evaluation for planetary rovers based on dynamic mobility index. In: *Procs of the 2011 IEEE/RSJ IROS*, pp.601-606.

[3] Sutoh M, et al (2015) The right path: comprehensive path planning for lunar exploration rovers. *IEEE RAM*. 22-33.

[4] Creager C, et al (2016) Effect of angle of attack on slope climbing performance. In: *Procs of the ASCE Earth and Space Conference* (in press).

[5] Wettergreen D, et al (2009) Design and field experimentation of a prototype lunar prospector. *IJRR*. 29 (12): 1551-1564.

[6] Wong JY (2008) *Theory of Ground Vehicles*, 4th edition. John Wiley & Sons Inc.

[7] Ishigami G, et al (2007) Terramechanics-based model for steering maneuver of planetary exploration rovers on loose soil. *JFR*. 24 (3): 233-250.

[8] Zhou F, et al (2014) Simulations of mars rover traverses. *JFR*. 31 (1): 140-160.

[9] Oravec H, et al (2010) Design and characterization of GRC-1: a soil for lunar terramechanics testing in Earth-ambient conditions. *J. Terramech.* 47: 361-377.